J Solid State Eletrochem (2004) 8: 147–158
DOI 10.1007/s10008-003-0434-4

ORIGINAL PAPER

**Benedetto Bozzini · Pietro Luigi Cavallotti
Ameriga Fanigliulo · Giuseppe Giovannelli
Claudio Mele · Stefano Natali**

Electrodeposition of white gold alloys: an electrochemical, spectroelectrochemical and structural study of the electrodeposition of Au-Sn alloys in the presence of 4-cyanopyridine

Published online: 14 January 2004

Abstract A bath for the electrodeposition of Au-Sn alloys is proposed and the properties of the deposit obtained have been studied, in view of applications in the field of white precious metal plating and electroforming. 4-Cyanopyridine has been employed as an organic additive to confer stability to the bath and compactness to the deposit. The electrochemical behaviour of the bath has been investigated by means of cyclic voltammetry, stripping potentiodynamic scans, open circuit potential decay measurements and potentiostatic transients. The nucleation behaviour of the system has been studied on glassy carbon electrodes. The electrodic behaviour of 4-cyanopyridine was investigated as a function of electrode potential by in situ Raman spectroscopy. The composition of the alloys was evaluated by electron dispersive spectroscopy, the crystalline structure by X-ray diffraction and the morphology by scanning electron microscopy. The effects of the additive on the crystalline structure and on the morphology of the electrodeposits have been highlighted. Potential-dependent adsorption, reorientation and cathodic reactivity of 4-cyanopyridine during the alloy electrodeposition process have been assessed.

Presented at the 3rd International Symposium on Electrochemical Processing of Tailored Materials held at the 53rd Annual Meeting of the International Society of Electrochemistry, 15–20 September 2002, Düsseldorf, Germany

B. Bozzini (✉) · A. Fanigliulo · C. Mele
Dipartimento di Ingegneria dell'Innovaz, INFM,
Università di Lecce, via Monteroni, 73100 Lecce, Italy
E-mail: benedetto.bozzini@unile.it
Tel.: +39-832-320325
Fax: +39-832-325004

P. L. Cavallotti
Dipartimento di Ingegneria Chimica,
Politecnico di Milano, via Mancinelli 7, 20131 Milan, Italy

G. Giovannelli · S. Natali
Dipartimento ICMMPC, Università di Roma I "La Sapienza",
via Eudossiana 18, 00185 Rome, Italy

Keywords Alloy electrodeposition · Au-Sn · 4-Cyanopyridine · Gold · Surface-enhanced Raman spectroscopy

Introduction

The electroforming of white precious metals and alloys is a non-trivial unsolved problem in applied electrochemistry. Systems so far tested to address this problem have revealed severe drawbacks, ranging from poor mechanical properties (Au-Ag alloys) to the impossibility of obtaining thick deposits (Pt) [1]. Apart from electroforming, as far as thin white precious metal decorative plating is concerned, the commercially viable processes require improvement. The traditional solutions are the electrodeposition of Rh, Au-Ni and Au-Pd. Rh plating is a reliable process, the metal has a perfectly white colour but its price has been considerably growing recently; Au-based alloys are therefore a good alternative. Au-Pd enjoyed considerable attention in the past, but the increase of the price of Pd eventually rendered the cost of the alloying element higher than that of Au. Au-Ni is the replacement of choice, but the well-known allergy problems tend to limit its application as a finishing layer [2]. The field of white metal electroforming and plating therefore appears to be wide open to innovation. A peculiar niche of remarkable expansion potential is 18-carat white gold electrodeposition.

Apart from the patent literature [3, 4, 5], the number of reports on the electrodeposition of Au-Sn alloys is very limited. Recently, two deposition systems not containing free cyanide have been proposed. One of them is based on the sulfite–Au(I) complex [6, 7]. The other bath is cyano–Au(I) [8] complex solutions. Published results [6, 7] mainly stress bath chemistry, deposit morphology and achievable compositional range, with special emphasis on high carat alloys, but give no electrochemical or structural details.

The deposits obtained from $Au(CN)_2^-$ solutions [8] were polyphasic and their composition could be varied

by changing the current density. Preliminary unpublished results obtained in our group on the galvanostatic electrodeposition from an acidic $Au(CN)_4^-/SnCl_6^{2-}$ bath pointed out the formation of a single phase of approximately equiatomic composition in a rather large current density interval (10–40 mA cm^{-2}). This Au(III)-Sn(IV) acidic system is a promising one in that thick, hard deposits with reproducible composition and structure, as well as good chromatic properties, can be produced. Nevertheless, two major drawbacks still have to be coped with: (1) the matte finish and tendency to form powdery deposits; (2) the limited bath stability, leading to the formation of anodic slimes and to flocculation upon storage. Organic additives undergoing electrodic adsorption are frequently employed to cope with similar problems. A screening of several molecules hinted at the beneficial actions of 4-cyanopyridine (4-CP) for Au(I)- and Au(III)-based electrolytes.

In this paper we report on the molecular level actions of 4-CP in a Au-Sn electroplating system. This investigation deals with the electrochemical behaviour of the bath, the crystallographic structure of the deposits, the nucleation and growth of the alloy crystallites, the morphology of the electrodeposited alloy layers and their composition. These electrochemical and structural results have been correlated with the spectroelectrochemical results of in situ surface-enhanced Raman spectroscopy (SERS) measurements.

Experimental

The electrodeposition bath was prepared with the following metal contents: 5 g L^{-1} Au (as $KAu(CN)_4$), 75 g L^{-1} Sn (as $SnCl_4{\cdot}5H_2O$). The solution was acidified by use of HCl (to pH 1.0) and subsequently by H_2SO_4 (to pH 0.5). The concentration of 4-CP was 100 ppm, in the relevant experiments.

Cyclic voltammograms (CVs), potentiostatic transients (PSTs), open-circuit potential decay (OCPD) experiments and potentiodynamic stripping curves (PSCs) were recorded with a computer-controlled AMEL 5000 potentiostat. The working electrode (WE) was a AMEL 492/GC3 glassy carbon (GC) disk of 3 mm diameter. Before each measurement the GC was stripped chemically by immersion in aqua regia; an outstanding degree of reproducibility was obtained. Triplicate PSTs were measured. Duplicate CVs were run in test cases. The CVs were measured at a rate of 50 mV s^{-1} with an anodic terminal voltage of + 700 mV and various cathodic terminal voltages (CTVs). The counter electrode was a large-area Pt foil. In some instances, polycrystalline Au electrodes were employed; they had been subjected to a flame annealing conditioning procedure (described in [9], for example) before use for electrochemical measurements.

The reference electrode (RE) was an AMEL Ag/AgCl containing 3 M KCl separated from the electroplating solution by a porous ceramic insert. The RE tip was placed at a distance of ca. 5 mm from the WE. Ohmic corrections applied by the positive feedback method were considered, but proved irrelevant due to the high conductivity of the solution. Potential values are reported vs. Ag/AgCl. The cathodic and anodic compartments of the cell were divided by a glass frit.

Alloy samples for structural, compositional and morphological studies were electrodeposited potentiostatically at −300, −500, −600 and −700 mV from solutions without and with 4-CP onto X-ray amorphous Ni-P (9% P) layers of thickness 30 μm, prepared as described [10]. The electroplating time was 60 min for potentiostatic electrodeposition at −300 and −500 mV and 30 min for −600 and −700 mV. The electrodeposition current densities (mean and one standard deviation) are reported in Table 1. For a given electrode potential, lower current densities are measured for the bath containing 4-CP. Notwithstanding the concurrent 4-CP reduction reaction (see section on SERS below) the inhibiting action of the adsorbed organic species dominates the integral current density.

Structural characterization was performed by XRD, using a Philips PW 1830 diffractometer equipped with a Philips PW 1820 combined vertical powder and thin-film goniometer and a Philips 1710 control unit. The adopted scan rate was 1 deg s^{-1}. The employed radiation was unmonochromated Cu Kα.

The morphology of the samples was studied with a Cambridge Stereoscan 360 SEM. The electron source was LaB_6. Electron detection was carried out with a scintillation photodetector. The typical working pressure was 10^{-7} mbar. Quantitative analysis of the sample composition was performed by EDS in the same vacuum chamber and with the same electron source as SEM with a Li-doped Si detector.

The SERS work was carried out with a LabRam confocal Raman system. Excitation at 632.8 nm was provided by a 12 mW He-Ne laser. A 10× long-working-distance objective was used. In situ electrochemical measurements were performed in a cell with a vertical polycrystalline Au disc working electrode of diameter 3 mm embedded into a Teflon holder. A metallographic polishing procedure, consisting of wet polishing with 1200 grit SiC paper, proved adequate for an excellent reproducibility of the spectro-electrochemical measurements. The counter electrode was a Pt wire loop (1.25 cm^2), concentric with the working electrode disk and the reference electrode (Ag/AgCl). The reference electrode probe tip was located 3 mm from the rim of the working electrode disk. We scanned the potential in the range 1000 mV to −500 mV, in the cathodic going direction.2

Results and discussion

Electrochemical results

Cyclic voltammetry

Calibration experiments with supporting electrolyte and Au(III) solution Calibration CVs were measured with

Table 1 Characteristics of Au-Sn electrodeposited layers and electrodeposition processes as a function of potentiostatic polarization and of the presence of 4-CP in the bath

Electrodeposition potential (mV vs. Ag/AgCl)	Addition of 4-CP	Current density (mean ± s.d.) (mA cm^{-2})	Au content (at%)	Crystalline structure
−300	No	−6.38 ± 0.91	100	Au
−500	No	−11.6 ± 0.30	49.33	AuSn
−600	No	−25.0 ± 2.9	32.81	AuSn, $AuSn_2$, $AuSn_4$
−700	No	−57.9 ± 4.5	53.84	AuSn
−300	Yes	−4.03 ± 0.88	100	Au
−500	Yes	−7.86 ± 0.42	89.53	Au_5Sn
−600	Yes	−13.9 ± 0.26	37.92	AuSn, $AuSn_2$, $AuSn_4$
−700	Yes	−44.2 ± 2.5	48.64	AuSn

the GC electrode in the supporting electrolyte; a very extended double-layer charging interval was observed, and a very high HER overvoltage was measured, as expected (~1200 mV, see Fig. 1, curve A). The electrode behaviour of 4-CP in the absence of Au(III) and Sn(IV) was also tested in this electrolyte by adding 2 g L^{-1} of the compound.

CVs were measured on both GC and polycrystalline Au electrodes. 4-CP displays a rich CV scenario related to adsorption and reaction on both GC and Au. The voltammetric details of the adsorption behaviour basically confirm previous results [11] and will not be discussed here, for the sake of compactness. We just report briefly on the cathodic reactivity of 4-CP. Wide-scan CVs for both electrode materials are shown in Fig. 2. The cathodic reactivity of 4-CP can be clearly assessed; the voltammetric feature relating to the reduction of this molecule can be effectively separated from the HER background by use of the GC electrode. The irreversible cathodic peak measured with the GC electrode can be explained with a reductive decomposition reaction giving rise to the formation of pyridine (actually pyridinium at the relevant pH) and hydrocyanic acid (see [11, 12] and our SERS data reported below).

The voltammetric behaviour of $Au(CN)_4^-$ in the supporting electrolyte is shown in Fig. 1. Curve A reports the voltammogram for the supporting electrolyte, for comparison. Curve B is the first scan performed with a clean GC electrode. Scans C are the ones following scan B. It can be observed that Au can be deposited at potentials less cathodic than the HER value for clean GC. After a given surface coverage with Au nuclei is attained, the HER occurs along with the electrodeposition of Au. Curve B displays a nucleation loop; the anodic going scan shows some HER-related fluctuations. The absence of nucleation features and the serration in the cathodic current density plots in curves C confirm this view.

Experiments with the Au(III)/Sn(IV) electrodeposition solution The salient features of the voltammetric behaviour of the Au-Sn alloy, both in the absence and in the presence of 4-CP, can be gleaned from Figs. 3, 4, 5 and 6, 7, 8, respectively. The insets in Figs. 3 and 6 show CVs measured with different cathodic terminal voltages, but the same anodic terminal voltage, proving that a different stripping behaviour is obtained by varying this parameter. The main plots in Figs. 4 and 7 report CVs measured with a high current density resolution, in order to better resolve the relevant sequence of cathodic and anodic peaks. Under these recording conditions the

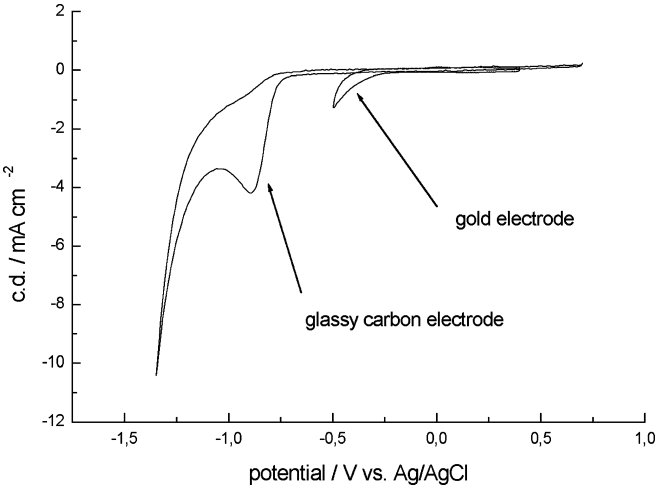

Fig. 2 CVs of 4-CP (100 ppm) at GC and polycrystalline gold electrodes, in the supporting HCl/H_2SO_4 electrolyte (pH 0.5). Scan rate: 50 mV s^{-1}

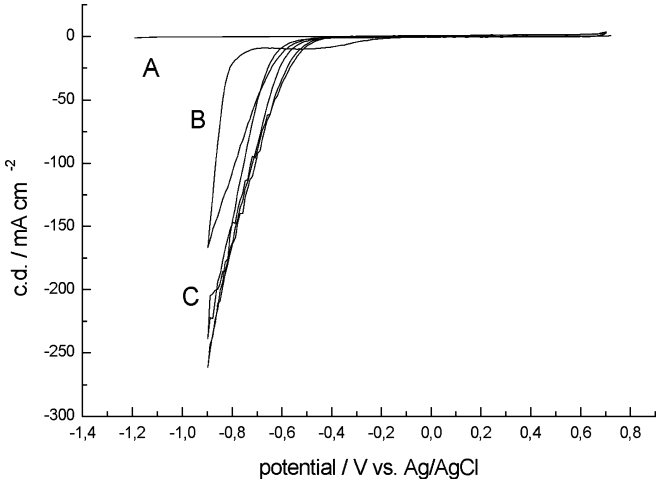

Fig. 1 CVs of a GC electrode in the supporting HCl/H_2SO_4 electrolyte (pH 0.5) (*A*) and in the same with addition of 5 g L^{-1} $KAu(CN)_4$ (*B*, *C*). Curve *B*: first cycle on a clean GC electrode. Curve *C*: the following cycles, displaying nucleation features. Scan rate: 50 mV s^{-1}

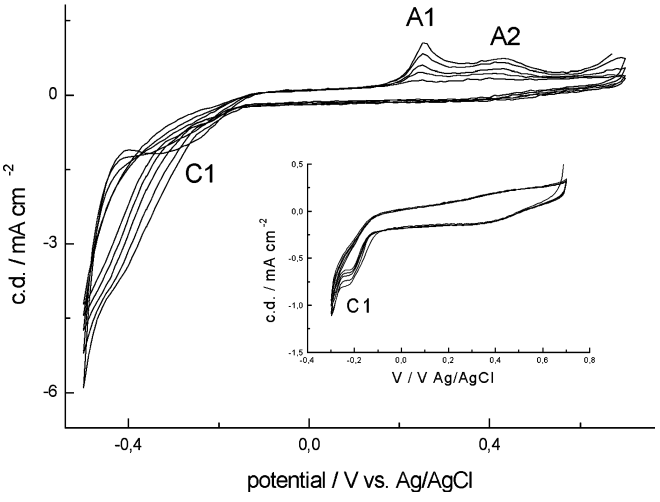

Fig. 3 CVs of the Au(III)-Sn(IV) alloy electrodeposition bath at a GC electrode. Scan rate: 50 mV s^{-1}. Cathodic terminal voltages: *main plot* −500 mV vs. Ag/AgCl; *inset* −300 mV vs. Ag/AgCl

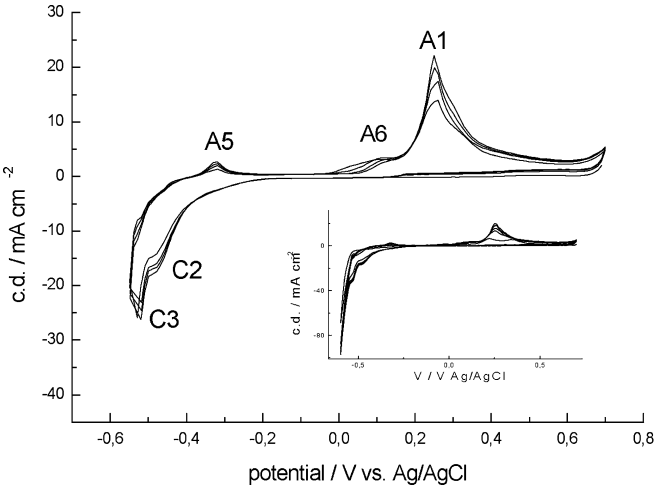

Fig. 4 CVs of the Au(III)-Sn(IV) alloy electrodeposition bath at a GC electrode. Scan rate: 50 mV s^{-1}. Cathodic terminal voltage: −600 mV vs. Ag/AgCl. The *main figure* exhibits a voltammogram recorded with a high current resolution; in these conditions the current density values saturate at the highest cathodic potentials and cannot be visualized. A full-scale, lower-resolution voltammogram is shown in the *inset*, displaying the full potential and current density range spanned in the experiment

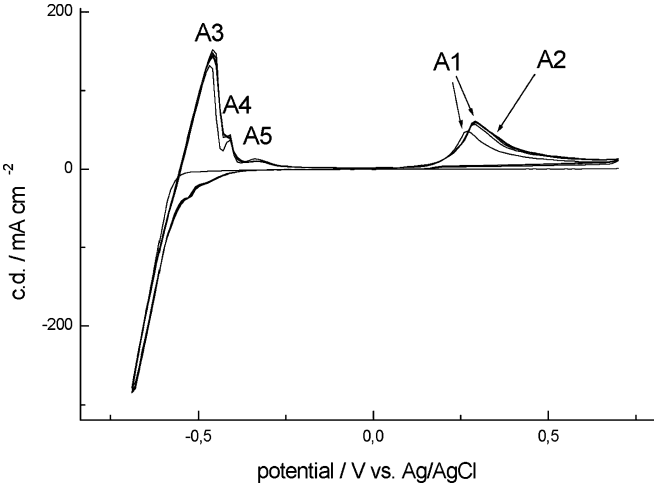

Fig. 5 CVs of the Au(III)-Sn(IV) alloy electrodeposition bath at a GC electrode. Scan rate: 50 mV s^{-1}. Cathodic terminal voltage: −700 mV vs. Ag/AgCl

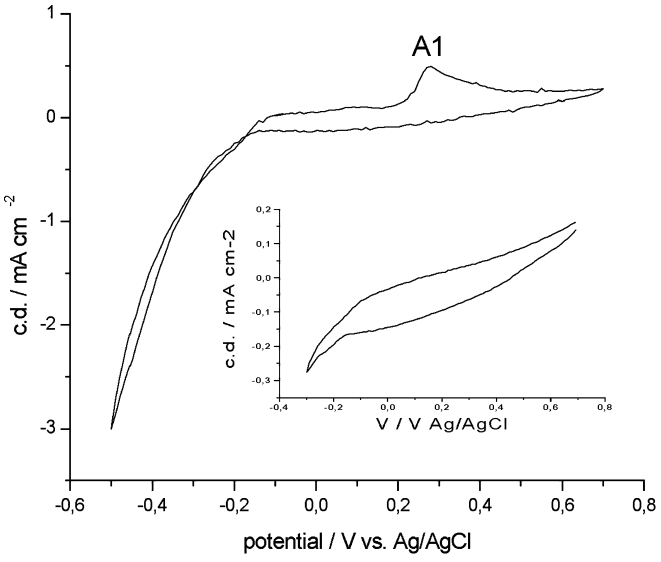

Fig. 6 CVs of the Au(III)-Sn(IV) alloy electrodeposition bath with 100 ppm 4-CP at a GC electrode. Scan rate: 50 mV s^{-1}. Cathodic terminal voltages: *main plot*, −500 mV vs. Ag/AgCl; *inset*, −300 mV vs. Ag/AgCl

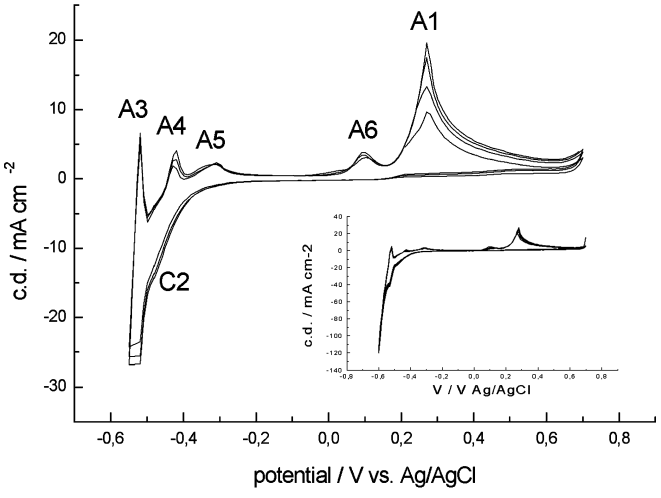

Fig. 7 CVs of the Au(III)-Sn(IV) alloy electrodeposition bath with 100 ppm 4-CP at a GC electrode. Scan rate: 50 mV s^{-1}. Cathodic terminal voltage: −600 mV vs. Ag/AgCl. The *main figure* exhibits a voltammogram recorded with a high current resolution; in these conditions the current density values saturate at the highest cathodic potentials and cannot be visualized. A full-scale, lower-resolution voltammogram is shown in the *inset*, displaying the full potential and current density range spanned in the experiment

current meter saturates and the current densities corresponding to the highest scanned cathodic potential values cannot be visualized. The full-scale, lower-resolution voltammograms are shown in the insets, for reference.

The most prominent voltammetric peaks as a function of CTV for the two solutions are given in Table 2. Of course, the details of the peak positions depend on the scan rate and number of scan repetitions (a more detailed discussion of this topic is beyond the scope of this paper) and the visibility of peaks may be a matter of current resolution.

Previous CV work in our group on similar alloys [8] and literature reports on the anodic behaviour of Au in acid solutions (e.g. [13]) provide guidelines for the assignment of the voltammetric features observed in this research. As already commented [8], the stripping (anodic going scan) curves are particularly informative. This feature is further enhanced in the investigated case by the use of the GC electrode. In addition, we carried out OCPD and PSC measurements in order to achieve a more conclusive insight regarding specific peaks. The interpretations of related groups of voltammetric peaks are listed below.

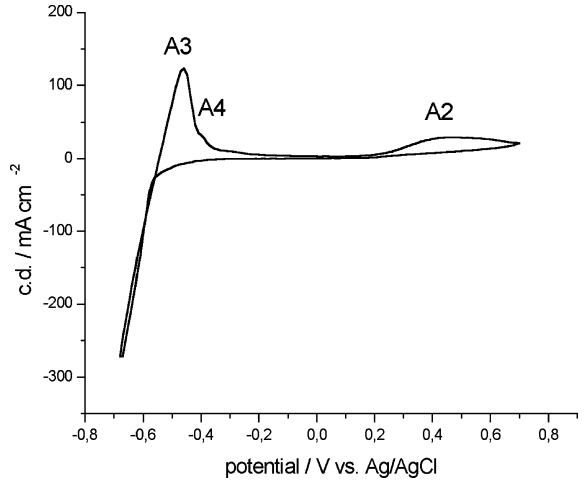

Fig. 8 CVs of the Au(III)-Sn(IV) alloy electrodeposition bath with 100 ppm 4-CP at a GC electrode. Scan rate: 50 mV s^{-1}. Cathodic terminal voltage: −700 mV vs. Ag/AgCl

1. A1 (Figs. 3, 4, 5, 6, 7), A2 (Figs. 3, 5, 8), A6 (Figs. 4, 7). These peaks can be attributed to the stripping of Au-rich phases. This conclusion is based on two pieces of evidence. (1) A comparison of the CVs measured in the Au (Fig. 1) and Au-Sn (Figs. 3, 4, 5) solutions shows that peaks of this kind do not appear in the absence of Sn. (2) PSC curves show these peaks as the only residual stripping features surviving prolonged OCPD. A PSC is shown in Fig. 9, corresponding to a deposit prepared by galvanostatic deposition at 45 mA cm^{-2} for 120 s from the Au-Sn bath containing 4-CP onto GC (whose OC potential in the relevant solution is +460 mV). Similar curves were recorded for other electrodeposition current densities and the behaviour is invariably of this kind; we omit them for brevity. Anodic peaks in this range of potentials appear to be ubiquitous. According to the crystallographic data reported below, they cannot be conclusively assigned to a specific type of phase electrodeposited at the CTV. Nevertheless, it is worth observing that single-phase Au_5Sn (with 4-CP, −500 mV) and AuSn (without 4-CP, −500 mV) deposits display only this kind of stripping peaks. Regardless of the compositional and structural details, the stripping of Au-Sn phases seems to occur by a selective dealloying process. The details of peak positions and peak multiplicity can be related to the phase structure of the deposits, but this analysis is beyond the scope of the present paper.
2. A3 (Figs. 5, 7, 8), A4 (Figs. 5, 7, 8), A5 (Figs. 4, 5, 7). In the Au(I)-Sn(IV) system, similar peaks have been attributed to the oxidation of Au-Sn alloys [8]. In the present systems, they can be related to Sn-rich phases. These peaks are in fact observed in electrodeposits in which either large (−600 mV without and with 4-CP) or trace amounts (−700 mV without and with 4-CP) are found of the $AuSn_2$ and/or $AuSn_4$ phases. The multiplicity of the peaks can again be related to selective corrosion processes. Further proof of this was obtained by performing OCPD measurements immediately after galvanostatic deposition. These measurements exhibit an astonishing reproducibility. A typical example, corresponding to galvanostatic electrodeposition at 45 mA cm^{-2} for 120 s in the alloy bath containing 4-CP, is shown in Fig. 10. From this figure it can be noticed that, as time elapses and corrosion proceeds, the electrode takes on a series of corrosion potentials. The sequence of potentials very closely follows the series of CV peak positions. The effectiveness of stripping at the OCP in the electrodeposition solution is proved by comparing PSCs measured immediately after plating and after the OCPD (Fig. 9).
3. C1 (Fig. 3). This peak can be tentatively assigned to the reduction of Sn(IV) to Sn(VI), as confirmed by EDX data revealing that no Sn is present in the electrodeposits obtained at −300 mV, at least after removal from the plating solution at the electrodeposition potential. The suppression of this peak in the system containing 4-CP can be explained by adsorbate-induced inhibition of this electrodic reaction. This fact might be related to the stabilization of a low-Sn phase, such as Au_5Sn, in the bath containing 4-CP at relatively low cathodic overvoltages (−500 mV).
4. C2 (Figs. 4, 7), C3 (Fig. 4). These peaks appear exclusively in the Sn-containing bath and can be related to the formation of Au-Sn alloys of different compositions, in close analogy with previous work [8].

The addition of 4-CP alters the voltammetric behaviour of the Au-Sn bath sizably. Adsorption of the

Table 2 Synopsis of voltammetric features as a function of cathodic terminal potential and of the presence of 4-CP in the bath

Cathodic potential (mV vs. Ag/AgCl)	Added 4-CP	Voltammetric peaks and respective positions (mV vs. Ag/AgCl)
−300	No	C1 (−200)
−500	No	C1 (−215), A1 (260), A2 (430)
−600	No	C2 (−470), C3 (−530), A3 (−530), A4 (−440), A5 (−320), A6 (100), A1 (250)
−700	No	C3 (−530), A3 (−460), A4 (−410), A5 (−330), A1 (295), A2 (430)
−300	Yes	No peaks visible
−500	Yes	A1 (280)
−600	Yes	C2 (−470), A3 (−520), A4 (−420), A5 (−320), A6 (100), A1 (270)
−700	Yes	A3 (−460), A4 (−400), A2 (500)

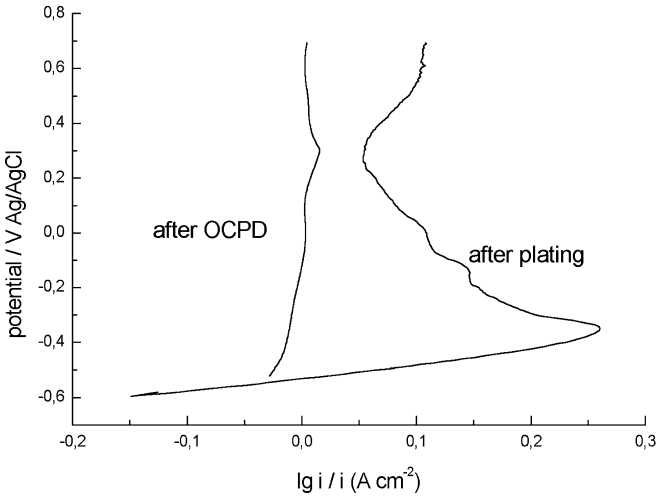

Fig. 9 Potentiodynamic stripping curve of a deposit prepared by galvanostatic deposition at 45 mA cm^{-2} for 120 s from the Au(III)-Sn(IV) bath with 100 ppm 4-CP onto GC and stripped in the same solution

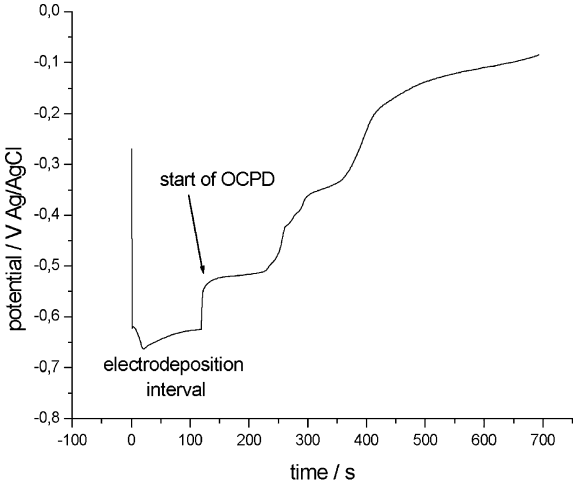

Fig. 10 OCPD curve for a deposit prepared by galvanostatic deposition at 45 mA cm^{-2} for 120 s from the Au(III)-Sn(IV) bath with 100 ppm 4-CP onto GC and corroded at open circuit in the same solution

additive gives rise to a general depression of the voltammetric loops and features, especially in the cathodic-going scan: only peak C2 (Figs. 4, 7) is discernible in the CV with CTV at −600 mV. Peaks A2 (Figs. 3, 5, 8), A3 (Figs. 5, 7, 8) and A4 (Figs. 5, 7, 8) can be clearly seen in both alloy baths, but their positions are slightly shifted between the two systems.

Potentiostatic current transients

PSTs were measured for cathodic potentials in the range −300 to −1250 mV in order to study the nucleation behaviour of the alloy systems of interest on GC electrodes. For comparison, the nucleation of Au from the same supporting electrolyte has also been studied.

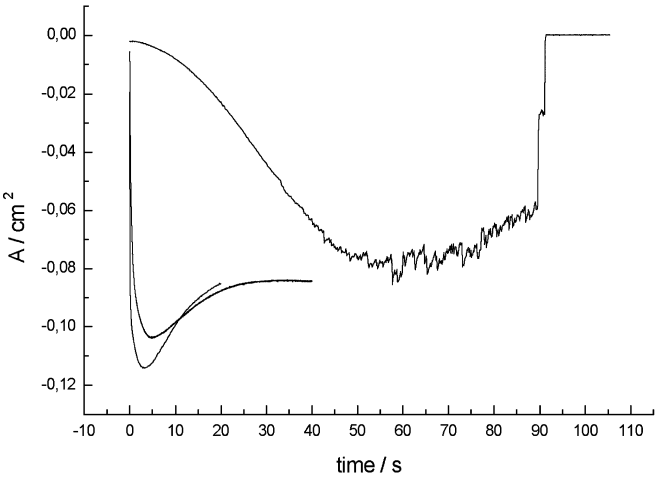

Fig. 11 Potentiostatic current transient curves measured at −600 mV vs. Ag/AgCl for Au(III), Au(III)-Sn(IV) and Au(III)-Sn(IV) with 100 ppm 4-CP

The rising portion of the transients is invariably in reasonable agreement with instantaneous or progressive nucleation models, but the descending portion of the transients is often affected by concurrent electrodic phenomena. In particular, a serration due to hydrogen evolution is typically observed with the Au bath and a secondary current density rise due to outgrowth processes is noticed at high cathodic potentials in the Au-Sn systems. A clear nucleation maximum could not be measured below −600 V and −400 mV for the alloy and Au systems, respectively, even for prolonged electrolysis. This fact might hint at a layer-by-layer growth mode; crystallographic evidence (the presence of a new hexagonal phase of the kind first found elsewhere [17]) gives support to this view. A typical set of transients recorded at −600 mV are shown in Fig. 11.

From the time behaviour of the transients and from the position of the current density maxima, a rather clear-cut scenario arises. (1) The transients are much slower for Au than for the alloy. (2) 4-CP anticipates the current density maximum. It is worth noting that the differences in current density peak positions, measured with triplicate transients for the systems without and with 4-CP, are extremely reliable. (3) Only instantaneous nucleation can be observed in the alloy system. The fact that the presence of Sn stabilizes instantaneous nucleation, even at low cathodic potentials, can be interpreted in terms of the typically normal electrokinetic behaviour of Sn [14]. (4) A transition between progressive and instantaneous nucleation takes place around −800 mV in the Au electrodeposition process. This transition of mechanism might be related to the cathodic surface coverage, with cyanide released during Au reduction.

The transient data can be elaborated as described elsewhere [15] to estimate the saturation nuclei density N_s (cm^{-2}) for instantaneous nucleation and the nucleation rate AN_o (s^{-1}) for progressive nucleation. This approach is admittedly simplified and comparative, since

we use a very rigid model developed for metals to interpret the salient features of the nucleation of alloys in a range of compositions. The progressive nucleation rate for the Au system in the range −400 to −700 mV displays a semilogarthmic dependence on potential.

N_s values as a function of potential are reported in Fig. 12. N_s varies as a function of cathodic potential in a roughly exponential way, denoting the fact that the number of growing centres increases with increasing overpotential. For the alloy deposition system, at each investigated potential, N_s is higher in the presence of 4-CP, indicating a decrease in the critical dimensions of the nuclei [16], which might relate to the higher morphological compactness achieved in the presence of the adsorbed additive (see below).

Morphological and compositional studies

Crystalline structure

XRD measurements have been performed for layers electrodeposited potentiostatically at −300, −500, −600 and −700 mV from solutions without and with 4-CP. The choice of these potentials is based on the CV results and corresponds to CTVs giving rise to dramatic changes in the stripping behaviour, which is believed to correlate with the formation of different alloy phases.

The obtained crystal structures are summarized in Table 1. The chemical compositions measured by EDX, also included in Table 1, conform to the phase composition revealed by XRD. Several phases of the Au-Sn system could be electrodeposited from the investigated solutions as a function of cathodic potential. Apart from traces of a low-overvoltage structure, all the phases formed correspond to equilibrium structures of the relevant binary system. Reflection attribution is therefore carried out by comparison with the Powder Diffraction Files for the phases of interest. An insightful analysis combined with structure calculations of the peak pattern attributed to the rhombohedral Au_5Sn phase in the Powder Diffraction Files actually reveals that a more accurate attribution could be made to the high-temperature hexagonal ζ phase, but we do not mean to go into such details in this paper. The deposits obtained at −300 mV from both alloy baths display a dominating nanocrystalline Au bcc phase, with traces of the hexagonal new structure disclosed previously [17]. This hexagonal phase, with $a = 0.990$ nm and $c = 0.521$ nm, is probably formed during the initial stages of electrodeposition, as revealed by the comparison of thin-film and powder diffractograms. 4-CP seems to stabilize this hexagonal phase. A typical thin-film diffractogram from the solution not containing 4-CP is shown in Fig. 13. Minor quantitative effects of 4-CP can be noticed, as far as phase composition, preferred orientation and degree of nanocrystallinity are concerned. Single δ-phase AuSn layers can be obtained at −500 and −700 mV from the bath without 4-CP and at −700 mV from the bath containing 4-CP. A typical diffractogram of this structure is shown in Fig. 14 (powder diffractogram). The texture of this phase is affected by the deposition conditions: the deposit at −500 mV from the additive-free bath displays a (100) preferred orientation; the deposit at −700 mV from the same solution is disoriented; while the deposit at −700 mV from the 4-CP-containing solution exhibits a (110) preferred orientation. The presence of adsorbed organics seems to stabilize the growth of a textured deposit, probably owing to preferred adsorption on specific crystalline planes, as suggested for the case of an aromatic quaternary ammonium salt [18]. An insightful discussion of these structural variations is beyond the scope of this paper.

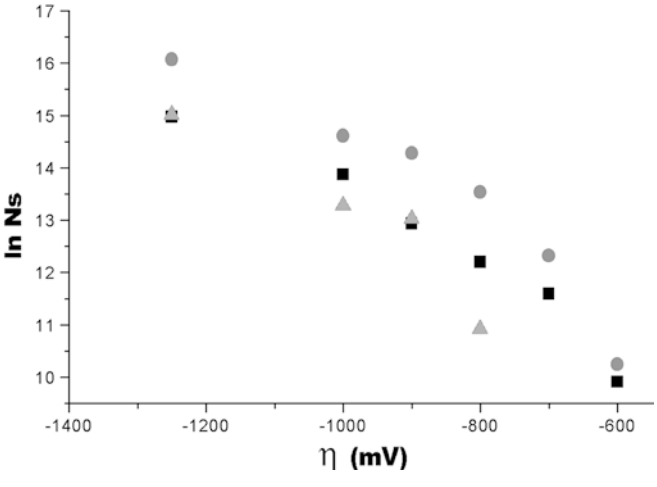

Fig. 12 Saturation nuclei density, N_s, for instantaneous nucleation as a function of potential for Au (*light squares??*), Au-Sn (*dark squares??*), Au-Sn + 4-CP (100 ppm) (*circles*)

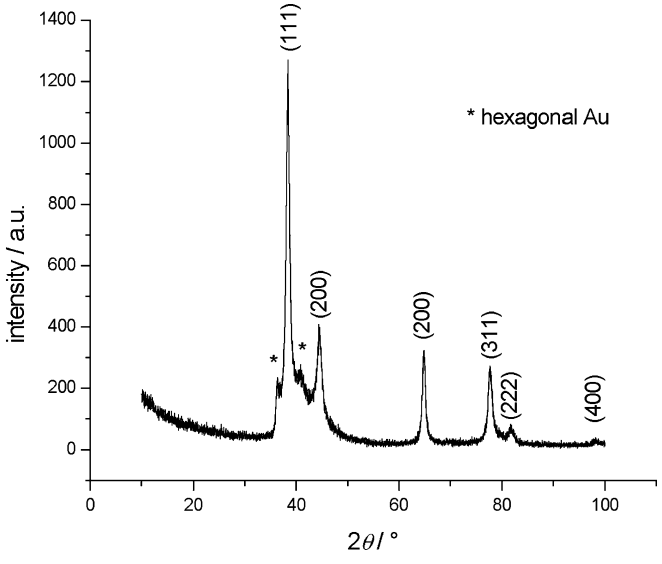

Fig. 13 Thin-film X-ray diffractogram of an electrodeposit grown from the Au(III)-Sn(IV) bath at −300 mV vs. Ag/AgCl

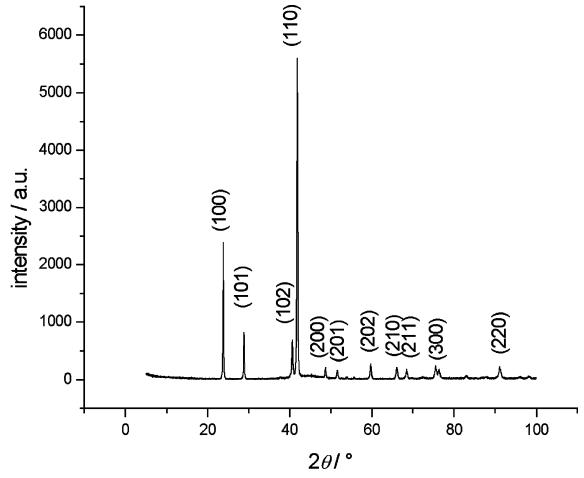

Fig. 14 Powder X-ray diffractogram of an electrodeposit grown from the Au(III)-Sn(IV) bath with 100 ppm 4-CP at −700 mV vs. Ag/AgCl

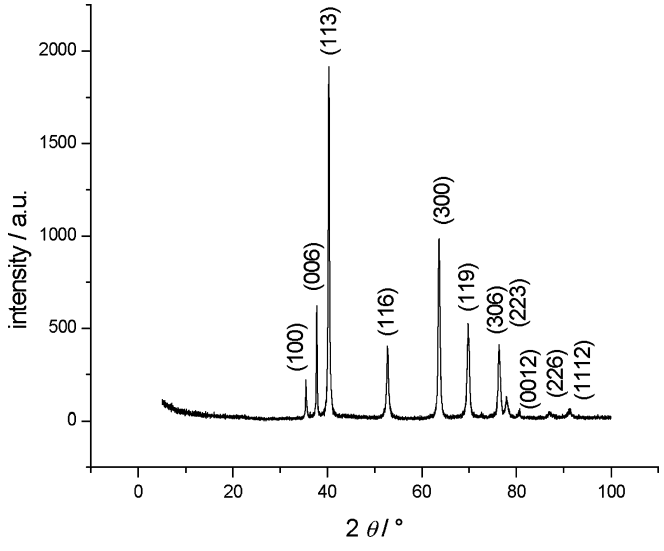

Fig. 15 Powder X-ray diffractogram of an electrodeposit grown from the Au(III)-Sn(IV) bath with 100 ppm 4-CP at −500 mV vs. Ag/AgCl

Layers grown from the solution containing 4-CP at −500 mV are single-phase Au_5Sn (Fig. 15, powder diffractogram). Coherently with voltammetric data, adsorbed 4-CP (see the section on SERS for details on reductive adsorption of 4-CP at this potential) seems to depress the reduction of Sn in this potential range. The electrodeposits obtained at −600 mV from both baths very reproducibly exhibit a transition condition in which a polyphasic structure is obtained, containing δ-AuSn, ϵ-$AuSn_2$ and η-$AuSn_4$. A typical thin-film diffractogram obtained from the additive-free solution is shown in Fig. 16. No qualitative effects of 4-CP can be recognized at this potential. Coherently with the phase composition, a decrease in Au content at this potential can be assessed by EDX (see Table 1), even though the current density regularly increases with cathodic potential.

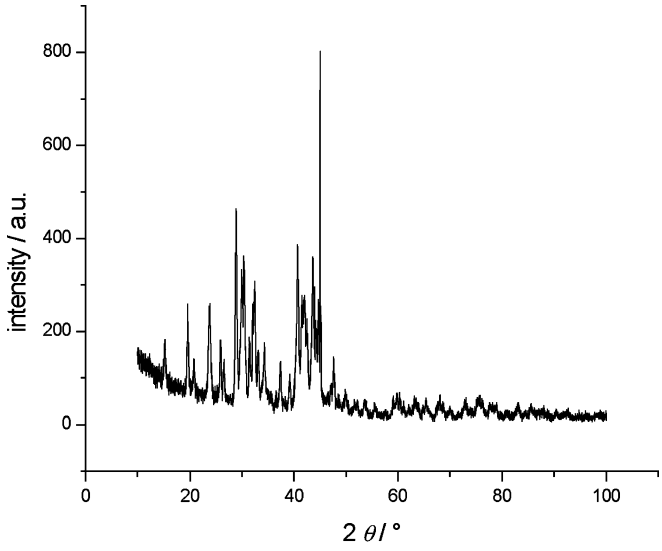

Fig. 16 Thin-film X-ray diffractogram of an electrodeposit grown from the Au(III)-Sn(IV) bath at −600 mV vs. Ag/AgCl

Morphology

The morphology of potentiostatically deposited samples has been studied by SEM as a function of cathodic potential for baths without and with 4-CP. The pure-Au layers obtained at −300 mV appear flat and featureless at the SEM, probably owing to lateral resolution limits. The coatings deposited at −500 mV for one hour exhibit acicular micrometric grains if grown from the additive-free solution (AuSn phase, Fig. 17, A-1) and smooth submicrometric humps from the 4-CP-containing bath (Au_5Sn phase, Fig. 17, A-2). The layers electrodeposited at −600 mV and displaying a three-phase structure show marked outgrowth features, including dendrites and leaves developing in the bath not containing 4-CP (Fig. 17, B-1). Electrodeposits obtained at the same potential from the 4-CP-containing bath show a much more compact morphology (Fig. 17, B-4). The morphologies of single-phase AuSn deposits obtained at −700 mV from baths without and with 4-CP are globular, with a tendency to outgrowth in the form of loose assemblies of globular grains (Fig. 17, C-1) and acicular grains (Fig. 17, C-2), respectively. In general it can observed that, from the morphological point of view, 4-CP tends to stabilize more compact growth forms. As pointed out in previous work on the effects of benzyldimethylphenylammonium chloride on Au electrodeposition [18, 19], the potential-dependent details of the crystallite shapes are expected to be related to the peculiarities of the adsorption behaviour of 4-CP and related electrolysis products on the different crystal faces of the growing crystallites.

In situ Raman experiments

SERS spectra have been recorded going from 1000 mV to −500 mV, spanning the potential range limited by

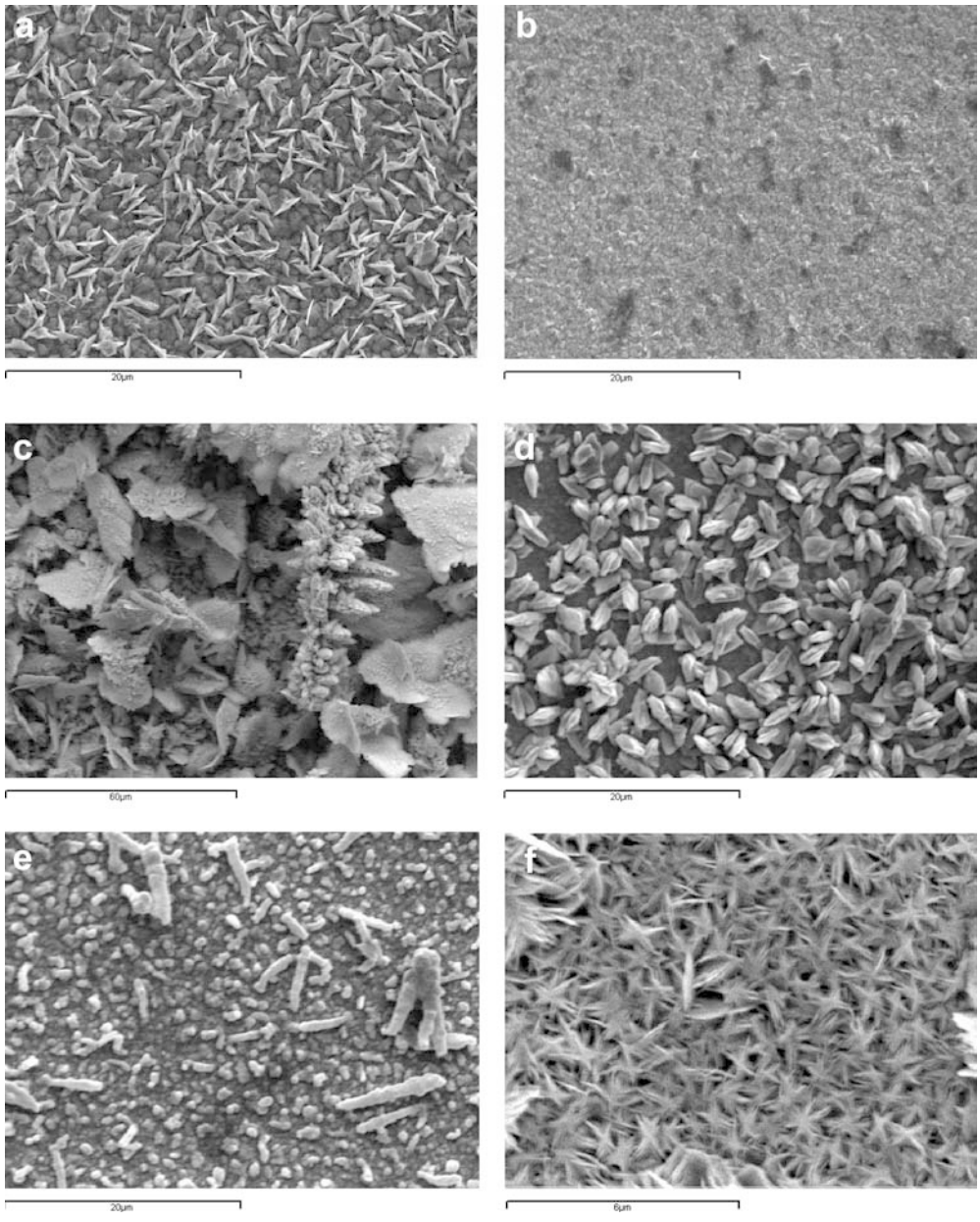

Fig. 17 SEM micrographs of electrodeposits from Au-Sn baths without (**a**, **c**, **e**??) and with (**b**, **d**, **f**??) 100 ppm 4-CP obtained at −500 mV (**a**, **b**??), −600 mV (**c**, **d**??) and −700 mV (**e**, **f**??). Potentials reported vs. Ag/AgCl

gold oxidation and alloy deposition, where the SERS effect is impaired by the presence of non-SERS-active tin.

Figures 18 and 19 show the spectra recorded as a function of potential. The band present at wavenumbers between 2123 and 2180 cm^{-1} in all the spectra reported in Fig. 19 is due to ν(CN) of the Au(III) cyano complex in several states. We will not deal with the spectroelectrochemistry of adsorbed cyanide in this report; a separate paper will be devoted to this topic. The band at 2203 cm^{-1} displayed in the spectra at 800 mV and (as a shoulder) at 1000 mV (Fig. 19) is due to cyanate, produced by oxidation of cyanide. The band present at 1102 cm^{-1} in the potential range −200 to 500 mV is due to the symmetric stretching of the sulfate ion, present in the solution used for SERS as supporting electrolyte and coadsorbed with 4-CP on the electrode surface at these potential values.

From Figs. 18 and 19 it can be observed that some vibrational bands revealing the presence of adsorbed 4-CP are present in all the potential range inspected (from 1000 to −500 mV); a list of the bands and of their assignments is given in Table 3 [12, 20, 21]. The spectra at potentials of 800 mV and higher (Fig. 18) show two major features: the C–N stretching band located at 2239 cm^{-1}, typical of 4-CP [12, 22], and the prominent (especially at 1000 mV) Au–N stretching band, located at ca. 260 cm^{-1} [19, 23]. From this evidence we can infer a vertical orientation of 4-CP, interacting with the metal surface through the N atom of the nitrile group. No additional vibrational features of the molecule, in particular those deriving from the aromatic framework, is

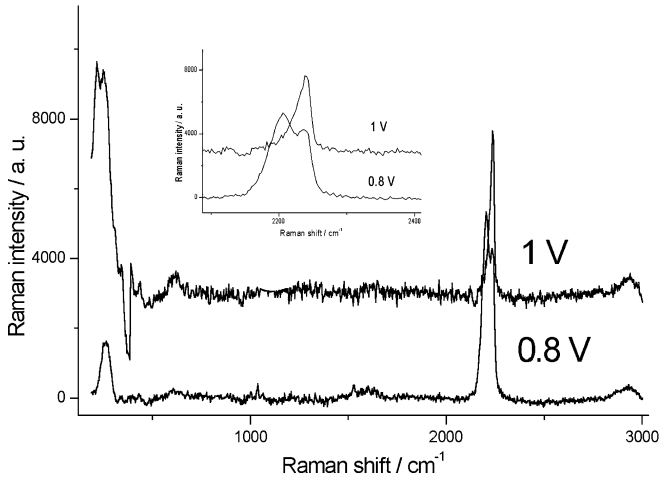

Fig. 18 Surface-enhanced Raman spectra of 4-CP at a poly-Au electrode, in the Au(III)-Sn(IV) bath, at 0.8 and 1 V vs. Ag/AgCl

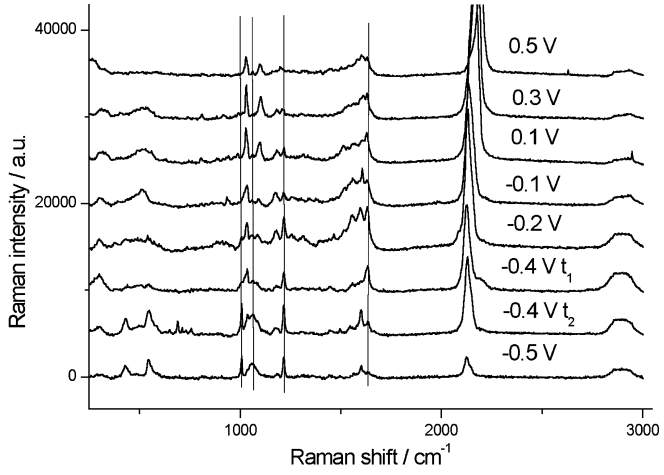

Fig. 19 Surface-enhanced Raman spectra of 4-CP at a poly-Au electrode, in the Au(III)-Sn(IV) bath, as a function of potential

apparent in these spectra, because of the dependence of SERS enhancement on the distance of the bonds from the surface. At potentials of 500 mV and lower (Fig. 19), the 4-CP C–N stretching is not present anymore, the Au–N peak greatly decreases in intensity and fades out below 300 mV, and vibrational aromatic features come out. These changes are compatible with a new orientation of the molecule, now interacting with the electrode via the aromatic ring. Whether the interaction occurs via the pyridine N lone pair (giving rise to a vertical orientation as well, but reversed with respect to the anodic domain) or via the π-electron system (resulting in a flat orientation) can be inferred by examining peak intensities and positions. In fact those modes are selectively enhanced in SERS which modify the polarizability components perpendicular to the plane of adsorption. These vibrations can be easily identified either by their symmetry group [24] or by the kind of deformation (in-plane or out-of-plane) they impose to the molecule [25].

Table 3 SERS vibrations of 4-CP. Band assignments after [9, 10, 18, 20]

Assignment	Symmetry	+1000 mV	+800 mV	+500 mV	+300 mV	+100 mV	−100 mV	−200 mV	−400 mV t1	−400 mV t2	−500 mV
C–H str.	a_1, b_2	2239	2239	2935–2873 w	2935–2850 w	2953–2850 w	2953–2850 w	2850–2945 m	2850–2945 m	2850–2945 m	2850–2945 m
C–N str.	a_1										
Ring str. (py)	a_1			1633 s	1633 s	1631 s	1636 s	1630 s	1636 s	1636 w	1637 w
Ring str.	a_1			1601 m	1610 m	1606	1607 s	1596 s	1599 w	1601 s	1605 s
Ring str.	b_2				1566 m	1560 m	1562 m	1558 m	1555 m	1551 m	1562 m
Ring str.	b_2			1501 w		1512 w	1522 w	1514 w		1501 w	
Ring str	b_1			1448 w				1466 w	1447 w		1443 w
C–H bend	b_2					1310 w	1379–1342–1305 w	1314 w			
X-sens	a_1						1259 m	1255 m			
C–H i.p. bend (py)	a_1			1204 w	1212 w	1218 w	1214 m	1216 s	1211 s	1214 s	1217 s
C–H i.p. bend	a_1				1180 w	1180 w	1177 m	1180 m		1180 m	1187 w
SO_4^{2-}				1102	1102	1099	1094 w	1086 w			
C–H i.p. bend	a_1							1057 w		1064 w	1072 s
Ring breath. (py)	a_1			1032 s	1031 s	1032 s	1033 s	1032 s	1031 s	1038 w	
Ring breath.	a_1							1003 w	1005 w	1004 s	1008 s
C–H o.p. bend	a_2			917 w	917 w	937 w	937 w				
C–H o.p. bend	b_1			809 w	810 w	806 w					
X-sens	b_2			566–446 w	565–463 w	563–460 w	514 m		554 s	556 s	548 s
X-sens	a_1									429	429
Au–N		256 s	261 m	265 w	321 w	307 w	301 w	301 w	301 m	301 w	301 w
Au–N (CN)											
Au–N (py)										223 w	223 w

Furthermore, a shift in the peak position may be indicative of charge transfer interactions [25]. Deeper inspection of the spectra reported in Fig. 19 reveals a continuous change in the band pattern developing in the cathodic direction. The shift of the ring breathing and ring stretching modes from 1032 to 1004 cm^{-1} and from 1637 to 1601 cm^{-1}, respectively, and the appearance of two out-of-plane deformation bands of 4-CP at 429 cm^{-1} and ca. 550 cm^{-1}, suggest that 4-CP is reorienting from a vertical to a flat configuration on going towards more negative potentials. Flipping of 4-CP between two vertical adsorption geometries on Au has been shown by SFG to occur through a flat adsorption state [22]. Such an intermediate flat configuration might be present between 800 and 500 mV. We did not collect specific data in order to ascertain this hypothesis, since we are mainly interested in the cathodic behaviour of this system. A minor complication of the spectra is caused by the presence of superimposed peaks due to the presence of traces of pyridine, reasonably formed by reduction of 4-CP at the counter electrode in the undivided SERS cell, during the initial anodic scan. The double peaks in the regions of ring breathing and ring stretching, the in-plane bending band at 1212 cm^{-1}, and the C–H stretching modes can be thus accounted for by the presence of pyridine, standing up on the electrode and interacting with it through the N atom in all the cathodic range investigated. This kind of orientation of pyridine at cathodic potentials is unexpected, since a flat π-bonded configuration has been reported in the literature (see e.g. [26, 27]). An insightful discussion of this interesting point is beyond the scope of this paper.

Several reasons can be put forward in an attempt at explaining these data, among which are: (1) electrode roughness and the attending effects on the relationship between IR and SERS surface selection rules; (2) co-adsorption [28]; and (3) concentration [29] contributions. The cathodic formation of pyridine is indeed directly observed by SERS from the increasing intensity of the band at 1212 cm^{-1} and the C–H stretching bands and from the fact that the bands due to an edge-on orientation of the aromatic ring (1637, 1032 cm^{-1}) do not completely vanish when 4-CP turns flat. The latter cited bands in pyridine and 4-CP differ by minor frequency shift [20, 30]. A time-resolved experiment has been carried out at −400 mV, a threshold potential for reorientation and reaction to occur. The results are summarized in Fig. 20. A sluggish kinetics of reorientation is found. The shoulder initially present at 2200 cm^{-1} and tending to disappear as the reaction time lapses has been attributed to a protonated form of 4-CP, resulting from the attack of H^+ on the nitrile moiety, thus weakening the triple bond [11]. This band can be initially observed because of the vertical orientation of the molecule and its fading out is indicative of the reorientation to the flat geometry taking place. The flat orientation favours the reduction of 4-CP, because the interaction via π-electrons makes the electron transfer from the metal to the molecule easier. The reductive degradation of 4-CP to pyridine and free cyanide has been suggested in the literature under neutral conditions [11, 12]; in this case, because of the acidic operating conditions, we believe that hydrocyanic acid instead of free cyanide forms as a counterpart of pyridine. In the asymptotic state (after 9 min), evidence of vertical pyridine is given by [20]: (1) C–H stretching at ca. 2800–3000 cm^{-1}; (2) ring breathing at 1032 cm^{-1}; and (3) ring deformation at 686 cm^{-1}. Furthermore, the peak attributed to Au–N stretching (301 cm^{-1}) progressively decreases in intensity with time, while a new peak at lower wavenumbers appears (223 cm^{-1}). The last observation can be interpreted as the co-presence of two kinds of Au–N bonds; the latter, lower frequency one, denotes a lower mass of the bonded molecule and is a suggestion of the formation of fresh pyridine on the electrode.

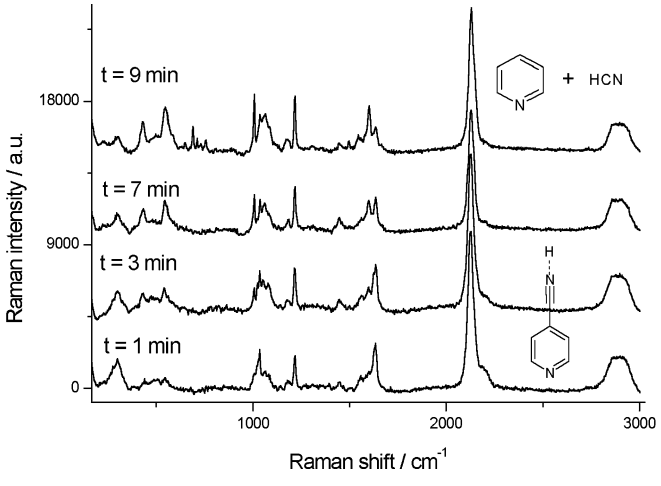

Fig. 20 Time-resolved surface-enhanced Raman spectra of 4-CP at a poly-Au electrode, in the Au(III)-Sn(IV) bath, at −400 mV vs. Ag/AgCl

Conclusions

A range of single-phase and multi-phase Au-Sn alloys can be electrodeposited galvanostatically from acidic $KAu(CN)_4$ and $SnCl_4{\cdot}5H_2O$ solutions. The presence of 4-CP in the alloy deposition bath correlates with the growth of different phases with specific textures as well as more compact morphologies. The codeposition of Sn is inhibited by 4-CP at the lower cathodic potentials. In particular, single-phase AuSn and Au_5Sn layers can be obtained at −500 mV from these solutions without and with additions of 4-CP, respectively. The formation of Au-Sn alloys can be detected by stripping voltammetry, exhibiting a selective dissolution pattern.

The formation of more compact morphologies relates to the effects of this additive on the nucleation process, as revealed by potentiostatic transients, adsorbed 4-CP stabilizing smaller nuclei in an instantaneous nucleation process.

The adsorption behaviour of 4-CP in the alloy bath in both the cathodic and anodic ranges has been studied by in situ SERS, revealing a reorientation from vertical nitrile-bonded in the anodic range to vertical pyridinic-N-bonded in the cathodic range at low potentials where only Au has been shown to deposit, to lying flat and reacting reductively, giving rise to pyridine and cyanide in the alloy deposition range. Molecular-level information on the conditions of the adsorbed additive during the growth process provides a framework for the rationalization and reconciliation of diverse characteristics of the alloy electrodeposition system, such as electrokinetics, nucleation, phase and chemical composition and mesoscopic morphology.

Acknowledgements Continuous and expert assistance with the electrochemical experiments is gratefully acknowledged to Mr. Francesco Bogani, Dipartimento di Ingegneria dell'Innovazione, Università di Lecce, Italy.

References

1. Bozzini B, Cavallotti PL (2000) Trans IMF 78:227
2. Bagnoud P, Nicoud S, Ramoni P (1996) Gold Technol 18:11
3. Zilske W (YEAR??) Electrolytic bath and process for the deposition of gold alloy coatings. US Pat 4,391,679
4. Stevens P (YEAR??) Tin-gold electroplating bath and process. US Pat 4,013,523
5. Zantini F (YEAR??) Electrodeposition of gold alloys. US Pat 3,764,489
6. Sun W, Ivey DG (1999) Mater Sci Eng B65:111
7. Sun W, Ivey DG (2001) J Mater Sci 36:757
8. Bozzini B, Giovannelli G, Natali S, Serra M, Fanigliulo A (2002) J Appl Electrochem 32:165
9. Fanigliulo A, Bozzini B (2002) Electrochim Acta 47:4511
10. Bozzini B, Cavallotti PL, Ivanov M, Arras L, Garbarino S, Terrenzio E, Visigalli P (1990) IEEE Trans Magn 26:45
11. Pluchery O, Clement V, Rodes A, Tadjeddine A (2001) Electrochim Acta 46:4319
12. Shi C, Zhang W, Birke RL, Lombardi JR (1997) J Electroanal Chem 423:67
13. Juodkazis K, Juodkazyte J, Juodiene T, Lukinskas A (1998) J Electroanal Chem 441:19
14. Cavallotti PL, Bozzini B, Nobili L, Zangari G (1994) Electrochim Acta 39:1123
15. Vargas T, Varma R (1991) In: Sarma XX??, Selam JR (eds) Techniques for characterization of electrodes and electrochemical processes. Wiley, New York, p 717
16. Trejo G, Gil AF, Gonzales I (1995) J Electrochem Soc 142:3404
17. Bozzini B, Giovannelli G, Natali S, Fanigliulo A, Cavallotti PL (2002) J Mater Sci 37:3903
18. Bozzini B, Fanigliulo A, Serra M (2001) J Crystal Growth 231:589
19. Bozzini B, Fanigliulo A (2002) J Appl Electrochem 32:1043
20. Green JHS, Harrison DJ (1977) Spectrochim Acta 33A:75
21. Topacli A, Bayari S (2001) Spectrochim Acta 57:1385
22. Pluchery O, Tadjeddine A (2001) J Electroanal Chem 500:379
23. Tadjeddine M, Flament JP (1999) Chem Phys 240:39
24. Creighton JA (1983) Surf Sci 124:209
25. Gao P, Weaver MJ (1985) J Phys Chem 89:5040
26. Pettinger B, Lipkowski J, Hoon-Khosla M (2001) J Electroanal Chem 500:471
27. Li N, Zamlynny V, Lipkowski J, Henglein F, Pettinger B (2002) J Electroanal Chem 542–525:43
28. Fanigliulo A, Bozzini B (2002) J Electroanal Chem 530:53
29. Fleishmann M, Hill IR (1983) J Electroanal Chem 146:353
30. Green JHS, Kynaston W, Paisley HM (1963) Spectrochim Acta 19:549